NANO LETTERS

2007
Vol. 7, No. 4
998−1002

Structural Phase Contrast in Polycrystalline Organic Semiconductor Films Observed by Broadband Near-Field Optical Spectroscopy

Robert Pomraenke,[†,‡] Claus Ropers,[†] Julien Renard,[†] Christoph Lienau,*[,†,‡] Larry Lüer,[§] Dario Polli,[§] and Giulio Cerullo*[,§]

Max-Born-Institut für Nichtlineare Optik und Kurzzeitspektroskopie, 12489 Berlin, Germany, Institut für Physik, Carl von Ossietzky Universität, 26111 Oldenburg, Germany, and ULTRAS-CNR-INFM, Dipartimento di Fisica, Politecnico di Milano, Piazza Leonardo da Vinci 32, I-20133 Milano, Italy

Received January 12, 2007; Revised Manuscript Received March 5, 2007

ABSTRACT

We demonstrate a novel near-field absorption spectrometer with 100 nm spatial resolution based on an ultrabroadband Ti:sapphire oscillator coupled to an aperture NSOM, enabling the measurement of nanoscale absorption spectra. The instrument is particularly suited for structural phase-selective imaging of organic materials at the nanoscale. We demonstrate that variations in the local absorption spectrum allow us to distinguish between the crystalline and the amorphous phases in polycrystalline phtalocyanine films, thus providing previously unavailable information on their mesoscopic texture.

Conjugated organic materials, also known as "organic semiconductors", combine the electronic and optical properties of semiconductors with the processing advantages and mechanical properties of plastics;[1] they have given rise to the field of "plastic electronics", with devices such as light-emitting diodes, lasers, photovoltaic cells, field-effect transistors, and all-organic integrated circuits.[2] A peculiar feature of organic semiconductors, as compared to inorganic ones, is structural inhomogeneity. It is very difficult to grow single crystals of size and optical quality good enough for applications; these materials, in the solid state, are generally amorphous or polycrystalline, with local order only achieved in mesoscopic domains with size ranging from a few tens to a few hundreds of nanometers.[3,4] In addition, many devices use blends of different molecules, which, due to the low entropy of mixing, undergo phase separation into domains of varying size and shape.[5] Many studies have proven that the size and type of these mesoscopic structures has a decisive influence on fluorescence quantum yield, charge carrier mobility and generation efficiency, parameters that must be fine-tuned against each other to optimize each kind of optoelectronic application.[6] Therefore, optimization of organic devices calls for an imaging method offering morphology contrast on the nanoscale.

Atomic force microscopy can distinguish domains of different heights, but cannot unambiguously assign them to different phases/molecular species due to its lack of chemical sensitivity. Optical spectroscopy is a powerful tool to resolve morphological changes thanks to the effects of the morphology on the local fluorescence/absorption spectra, but its spatial resolution is usually limited by diffraction to dimensions of the order of the wavelength. The NSOM allows one to overcome this limit by confining the light on the nanometer scale using a suitable probe. In the so-called aperture NSOM, a nanometer-sized aperture, usually realized by a metal-coated tapered optical fiber, confines the optical field in an evanescent, nonpropagating wave. The latter can be transformed into a propagating wave by interaction with a sample approached to the aperture at a distance much smaller than the wavelength (near field). An NSOM image is acquired by raster scanning the probe on the sample and is accompanied by a high-resolution topographic map. Typical spatial resolution of the aperture NSOM is ≈100 nm.

In its standard implementation, the NSOM is illuminated by a single laser wavelength, and the light transmitted/reflected by the sample or its fluorescence are collected by the detector.[7−11] In special cases, this allows for a clear

* Corresponding authors. E-mail: christoph.lienau@uni-oldenburg.de (C.L.); giulio.cerullo@fisi.polimi.it (G.C.).
[†] Max-Born-Institut für Nichtlineare Optik und Kurzzeitspektroskopie.
[‡] Institut für Physik, Carl von Ossietzky Universität.
[§] ULTRAS-CNR-INFM, Dipartimento di Fisica, Politecnico di Milano.

10.1021/nl070083i CCC: $37.00
Published on Web 03/27/2007

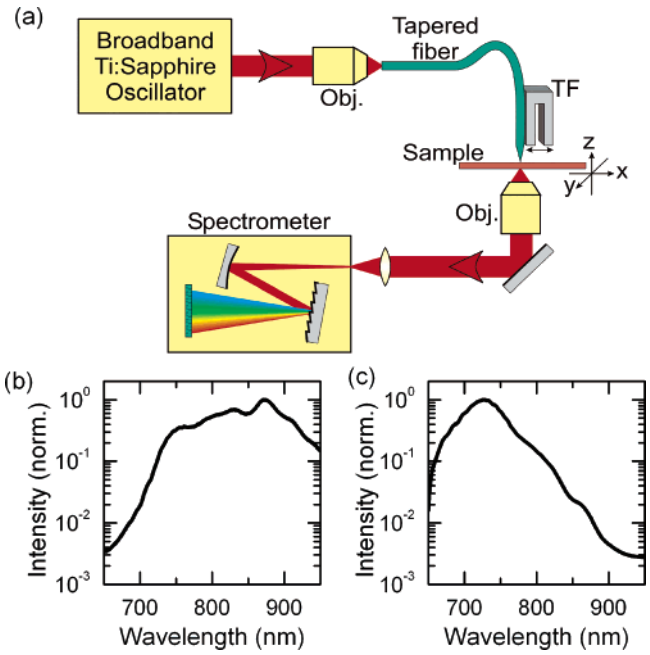

Figure 1. (a) Experimental setup of the spectrally broadband NSOM, (b) spectrum generated by the Ti:sapphire oscillator, and (c) spectrum transmitted through the metal-coated aperture probe.

interpretation by imaging prominent fluorescence wavelengths of known pure phases.[9−11] More generally, however, an unambiguous assignment of morphological phases requires the measurement of nanoscale absorption spectra. Such experiments are challenging because of the difficulty of generating broadband near-field illumination with sufficient intensity. Incoherent light sources (such as an arc lamp) emit broadband spectra,[12] but these can be coupled only with very poor throughput to the NSOM probe. On the other hand, femtosecond lasers provide spatially coherent ultrabroadband light beams, either directly from the laser oscillator or by supercontinuum generation, which can be efficiently coupled into the NSOM probe.[13,14]

Here, we report on a broadband near-field spectrometer based on an aperture NSOM coupled to an ultrabroadband Ti:sapphire laser. The system enables the measurement of nanoscale absorption spectra over the 650−950 nm wavelength range with sub-100 nm spatial resolution and discloses previously unavailable information on the nanoscale morphologic texture of organic semiconductors. We present a first application to the imaging of different structural phases of a polycrystalline thin film, showing spatial fluctuations of the phase composition on a 300 nm length scale, which are uncorrelated with the sample topography.

Figure 1a shows a schematic of the broadband NSOM. Illumination is provided by an ultrabroadband Ti:sapphire oscillator (Femtolasers model Femtosource Rainbow) generating 6 fs pulses with a spectrum ranging from 650 to 970 nm (see Figure 1b). A portion of the laser output is coupled to an Al-coated tapered optical fiber manufactured by the pulling method with a 50−100 nm aperture (Veeco, model no. 1730-00). The fiber tip is glued on a quartz tuning fork, which is used as a detector for shear-force tip−sample distance regulation. A constant tip−sample distance of 10 nm is maintained during scanning. We found that reliable NSOM operation, in terms of stability of the fiber coating and the tip−sample contact, was possible for coupled powers up to 10 mW, so that we chose to work at 3 mW. The sample is mounted on a linearized piezoelectric translation stage (Physik Instrumente P730.20) allowing $x-y$ scans with a range of up to 100 × 100 μm^2. The spatial resolution of the microscope was determined by calibration measurements on a test projection pattern and was found to be less than 100 nm before and after the actual measurements. The tip aperture showed no degradation during the course of the experiment. The light exiting the fiber tip illuminates the sample, and the transmitted light is collected by a 0.4-NA long working distance microscope objective and imaged onto the entrance slit of a spectrometer (Acton Spectra Pro 500i) equipped with a high-sensitivity liquid-nitrogen-cooled back-illuminated deep-depletion CCD detector. A typical transmitted light spectrum, for an integration time of 50 ms, is shown in Figure 1c: we achieve a count rate well above the dark current background for the entire 670−950 nm wavelength range. The overall smoothness of the spectrum makes it well-suited for transmission spectroscopy. By raster scanning the sample under the tip, it is possible to record the transmitted light spectrum at every sample position, $I_T^{sample}(\omega,x,y)$. Local absorption spectra are obtained by comparing $I_T^{sample}(\omega,x,y)$ to the spectrum of the light, $I_T^{glass}(\omega)$, transmitted through a transparent glass substrate held at a fixed distance of 10 nm from the near-field fiber probe, by computing the quantity:

$$A(\omega,x,y) = -\log\left(\frac{I_T^{sample}(\omega,x,y)}{I_T^{glass}(\omega)}\right)$$

Acquisition of the complete absorption spectrum at every sample position, rather than sequentially acquiring images at different wavelengths, speeds up the measurement, minimizing drifts in the experimental setup. In addition, it avoids possible morphological changes and photobleaching induced by multiple scans.

We use the NSOM spectrometer to image thin films of oxotitanyl phthalocyanine (TiOPc), which is a promising candidate for organic photovoltaics. Phthalocyanines (PCs) are particularly interesting among organic semiconductors because of their good photochemical and thermal stability, high photoconductivity, and excellent transport properties.[15−17] Depending on the molecular self-stacking ability and the thin film preparation procedure, PCs assume different forms, either crystalline or amorphous. TiOPc in its α-crystalline form (phase II) presents a particularly efficient charge photogeneration and a strong optical absorption in the red and near-IR spectral regions, so that a heterojunction with a good electron conductor that absorbs the remaining blue-green region can lead to highly efficient solar cells with complete coverage of the solar spectrum.[18−20] The phase transition from amorphous to crystalline in TiOPc thin films can be achieved by either thermal annealing[17,21] or vapor treatment with ethanol or tethrahydrofuran (THF).[15,21] The resulting films are polycrystalline, consisting of nanocrystallites interfaced by amorphous regions; the size and

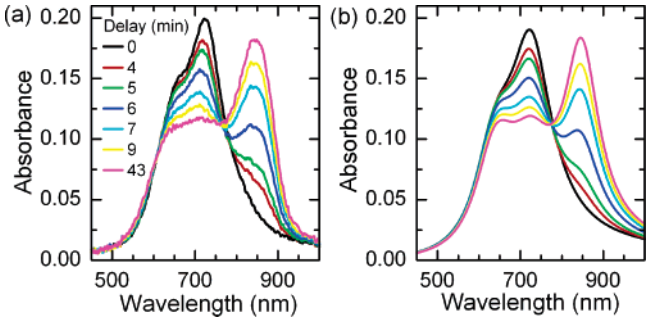

Figure 2. (a) Far-field absorption spectra of TiOPc thin films as deposited and after varying exposure times to THF atmosphere. The development of the crystalline phase is evidenced by the growth of the absorption band at 845 nm. (b) Calculated far-field spectra according to the three-resonances model described in the text.

spatial distribution of the crystallites, presently unknown, is a crucial parameter to determine the charge separation/recombination ratio.

TiOPc samples were prepared on glass slides by vapor deposition in high vacuum (base pressure 10^{-6} mbar) at an evaporation rate of about 2 Å/s to a thickness of ≈70 nm. Subsequent vapor treatment was performed in THF-saturated air at room temperature under simultaneous monitoring of the absorption spectrum. The growth of the crystalline phase II band started ≈2 min after the beginning of the treatment; conversion reached its stationary state after ≈20 min. Figure 2a shows as a black line the far-field absorption spectrum of an amorphous TiOPc film prepared by vapor deposition; it consists of the Q-band peaking at 720 nm, with a well-defined vibronic replica at 653 nm. Figure 2a also displays a sequence of absorption spectra of TiOPc during vapor treatment with THF. This sequence reveals the gradual formation of the crystalline phase II on a few minutes time scale, as evidenced by the development of a red-shifted absorption band, peaking at 845 nm, and the corresponding reduction of the 720 nm amorphous phase peak. The 845 nm peak, which is a spectroscopic signature of phase II,[15] has been attributed either to excitonic delocalisation induced by the formation of J aggregates in the crystalline phase[17] or to molecular distortion lifting the degeneracy of the fundamental electronic transition.[22] During the conversion, the shape of the spectrum reflects the simultaneous presence of the two phases. Conversion can be frozen at any time by removing the sample from the vapor chamber. The far-field spectra are satisfactorily reproduced by a model (detailed in the Supporting Information) in which the molecular transitions are described by a set of optical resonances, described for simplicity by Lorentzian lineshapes. Simulated far-field absorption spectra corresponding to the measured ones are shown in Figure 2b.

Using the broadband NSOM spectrometer, we measured spatially resolved absorption spectra of a partially converted TiOPc film, corresponding to 7 min vapor treatment (cyan line in Figure 2). Figure 3 shows absorbance images averaged over two different wavelength regions: 700−750 nm (b) and 820−900 nm (c), together with a topographic map (a). One clearly sees that some areas with higher absorption around 720 nm (amorphous phase peak) show less absorption around 845 nm (crystalline phase peak) and vice versa. This immediately evidences strong spatial fluctuations in the local composition of the sample resulting from pronounced structural phase disorder in the TiOPc film. No correlation can be established between topography and absorption images, demonstrating the absence of topographic artefacts[23] and indicating the unique power of broadband NSOM spectroscopy to reveal sample features that cannot be easily observed by other nonoptical approaches. We observe that some areas in the images show high or low absorption both in the 700−750 and 820−900 nm spectral ranges, indicating local fluctuations of the sample density, the orientation of the crystalline domains, and/or the thickness. Such absorption fluctuations would prevent an evaluation of local sample composition based on single-wavelength absorption images; on the other hand, our broadband approach allows removal of this ambiguity and distinguishing composition from absorption fluctuations.

Figure 3d shows measured near-field absorption spectra at four representative positions in the image (indicated by dots). The local spectra display dramatic changes with position, ranging from a nearly amorphous structure (positions C and D) to a nearly completely converted one (positions A and B). To model local absorption spectra, we used the same phenomenological approach as before (see Supporting Information), in which the transmitted light intensity is given by the superposition of the incident field and the electric field reemitted by the sample polarization. Unlike the far-field spectra, the near-field ones are expected to display an additional phase shift φ between incident and reemitted fields resulting from the spatially averaged phase differences between the fields emitted by the nanoaperture and the active material.[14,24] Because in the near-field retardation effects are weak, it is a good approximation to assume this additional phase shift as frequency-independent. To account for this, we introduced near-field phase shifts φ_{am} and φ_{cr} for the amorphous and crystalline phase emissions, respectively. We could reproduce the experimental spectra (dashed lines in Figure 3d) by introducing a small shift of $\varphi_{am} \approx 0.1$ rad for the amorphous phase emission and a slightly larger shift $\varphi_{cr} \approx 0.2$ rad for the regions with a predominantly crystalline composition. Such phase shifts allow us to reproduce the 10−15 nm spectral shifts of the crystalline peak between near- and far-field spectra. Both observed phase shifts are substantially smaller than the large shifts of $\varphi \approx \pi/2$ recently observed in the near-field spectrum of a single metal nanoparticle.[14] We essentially attribute this to the finite geometrical size of the crystalline and amorphous regions, which are much bigger than the 25 nm radius of the nanoparticle investigated in ref 14. From such fits to the near-field transmission spectra, we can thus directly extract the local crystalline phase molar fraction parameter β (defined in the Supporting Information), as indicated in Figure 3d for four different sample positions.

Figure 4a presents a spatial map of $\beta(x,y)$ for a sample with an average conversion β_{av} of 58% and a far-field spectrum indicated by the blue line in Figure 2: this map reveals extremely pronounced spatial fluctuations of the

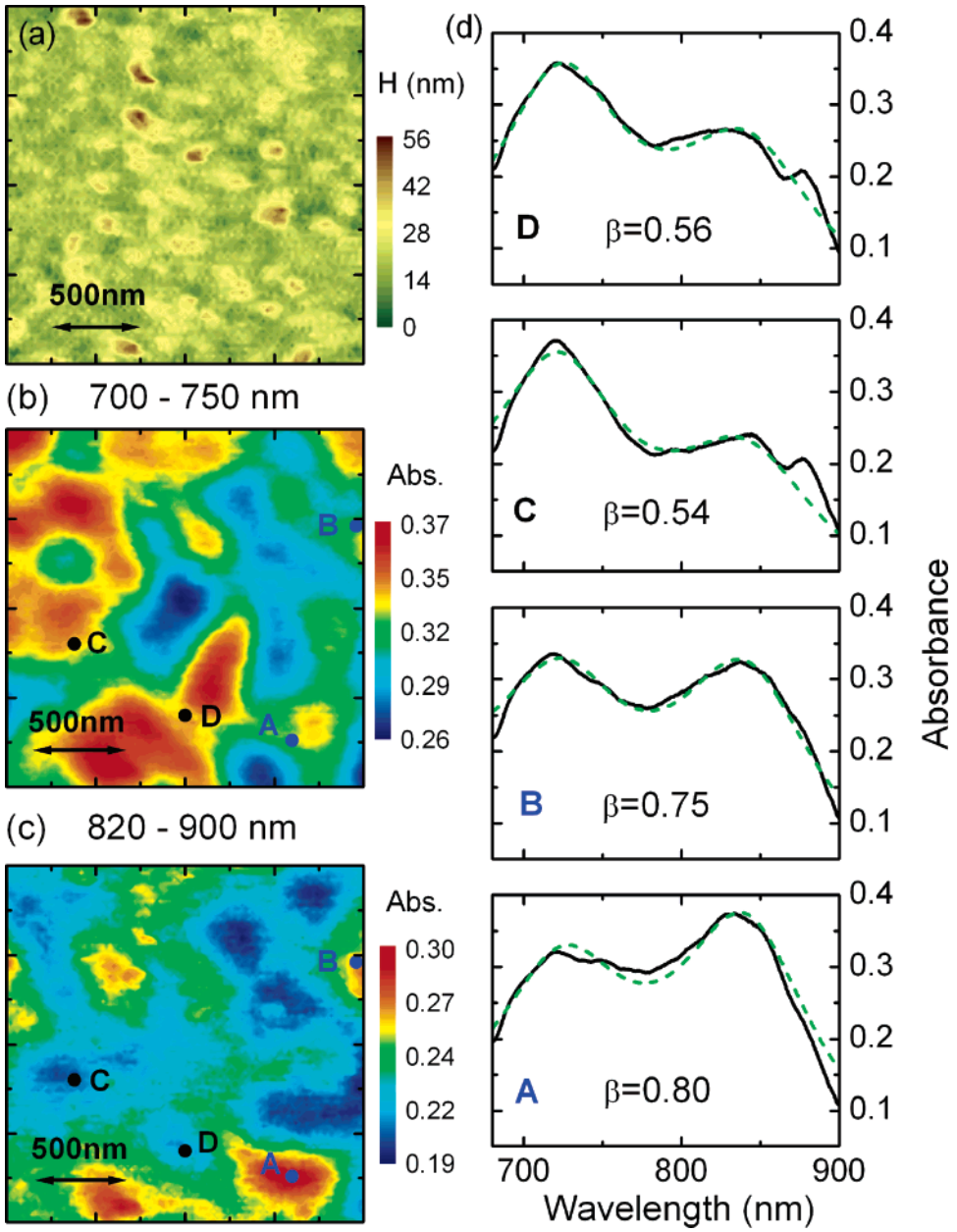

Figure 3. Spatially resolved absorption spectra of polycrystalline TiOPc films. Topography map (a) and optical absorbance maps in the 700−750 nm (b) and 820−900 nm (c) wavelength ranges. (d) Near-field absorption spectra at selected positions on the sample (solid lines) and fits according to the model presented in the text (dashed lines). The extracted crystalline phase molar fraction β is given as an inset.

structural composition, spanning essentially the entire β parameter range between 0 and 1. Similar spatial fluctuations on a length scale of 300−500 nm are found in samples with β_{av} of 32% (b) and 94% (c), yet with variation over a much narrower range. Two important observations about the structural composition in TiOPc films can be made: First, we observe, with the present 100 nm resolution, essentially the same range of composition parameters as in the far-field spectra (Figure 2) and no significant narrowing or spectral fluctuations of the absorption spectrum in the crystalline region. This points to an inhomogeneous broadening of the near-field spectra due to the presence of compositional disorder on a sub-100 nm scale. Therefore, even our near-field measurements effectively sample over composition fluctuations on a length scale below our optical resolution. Second, our results reveal changes of the local composition on a rather large spatial scale of several hundreds of nanometers, clearly above the resolution of our instrument. Within such composition islands, the optical properties are essentially given by the far-field spectra of a sample with the same average conversion parameter.

These findings present a possible handle to device optimization because they refer to both exciton separation and charge transport, crucial parameters in photovoltaics. The observed sub-100 nm compositional disorder is on the order of the exciton diffusion length, which can be as high as ≈70 nm, as recently measured in a similar material.[25] Hence, excitons generated in the amorphous zones should still be able to reach the crystalline zones of high separation efficiency. This effect can be exploited to enlarge the spectral

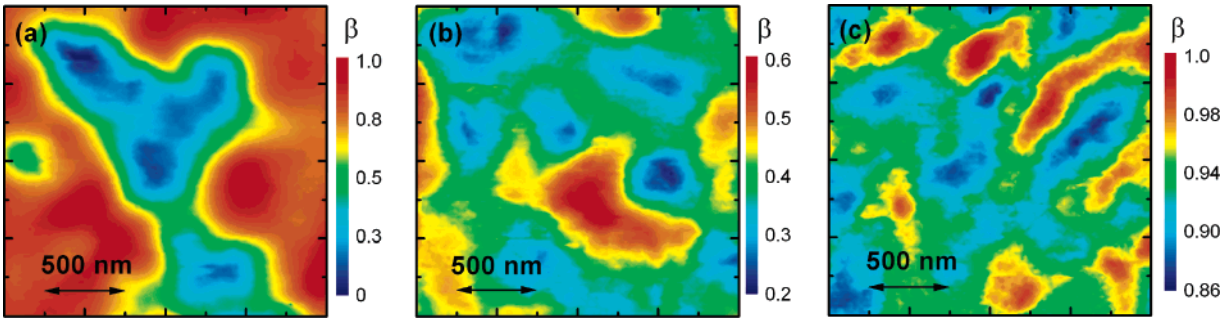

Figure 4. Crystalline phase molar fraction maps $\beta(x,y)$. The maps are extracted in three different samples with an average conversion of (a) $\beta_{av} = 0.58$, (b) $\beta_{av} = 0.32$, and (c) $\beta_{av} = 0.94$.

sensitivity of a single-component two-phase system. On the other hand, the correlation length of the composition parameter β, which is observed to be several hundreds of nanometers in our measurements, might inhibit charge percolation to the electrode in case of a clustering of the high charge mobility crystalline regions. In this case, charge recombination would be favored over charge transport. This knowledge can be used to optimize the film formation protocol and the electrode geometry in photovoltaic devices.

In conclusion, we have demonstrated a broadband near-field spectrometer, allowing the measurement of absorption spectra at the nanoscale. We apply this instrument to image the distribution of structural phases in a TiOPc thin film with 100 nm spatial resolution and evidence structural composition disorder on a scale comparable with the exciton diffusion length. Knowledge of the nanoscale spatial distribution of crystalline and amorphous phases represents an important tool for optimization of TiOPc-based photovoltaic devices. We believe that our instrument can allow new insight into the mesoscopic structure of organic materials by providing information not available with other techniques. The wavelength range of the spectrometer can be further extended both in the visible and the near-IR by supercontinuum generation in a microstructured fiber.[26] In addition, by using a scattering NSOM approach,[27] we envision an order of magnitude improvement in spatial resolution of absorption spectra, down to the 10 nm range, which is the characteristic size of excitons in organic materials.

Acknowledgment. The authors acknowledge support from the European Community-Access to Research Infrastructure Action of the Improving Human Potential Program, contract RII3-CT-2003-506350, from the Italian FIRB project "Nanotechnologies and Nanodevices for the Information Society" and from the Deutsche Forschungsgemeinschaft via the Sonderforschungsbereich SFB 296.

Supporting Information Available: Modeling of far-field and near-field absorption spectra. This material is available free of charge via the Internet at http://pubs.acs.org.

References

(1) Friend, R. H.; Gymer, R. W.; Holmes, A. B.; Burroughes, J. H.; Marks, R. N.; Taliani, C.; Bradley, D. D. C.; Dossantos, D. A.; Brédas, J. L.; Logdlund, M.; Salaneck, W. R. *Nature* **1999**, *397*, 121.
(2) Forrest, S. R. *Nature* **2004**, *428*, 911.
(3) Nguyen, T.-Q.; Martini, I. B.; Liu, J.; Schwartz, B. J. *J. Phys. Chem. B* **2000**, *104*, 237.
(4) Schwartz, B. J. *Annu. Rev. Phys. Chem.* **2003**, *54*, 141.
(5) Halls, J. J. M.; Walsh, C. A.; Greenham, N. C.; Marseglia, E. A.; Friend, R. H.; Moratti, S. C.; Holmes, A. B. *Nature* **1995**, *376*, 498.
(6) Sirringhaus, H.; Brown, P. J.; Friend, R. H.; Nielsen, M. M.; Bechgaard, K.; Langeveldvoss, B. M. W.; Spiering, A. J. H.; Janssen, R. A. J.; Meijer, E. W.; Herwig, P.; Deleeuw, D. M. *Nature* **1999**, *401*, 685.
(7) DeAro, J. A.; Weston, K. D.; Buratto, S. K.; Lemmer, U. *Chem. Phys. Lett.* **1997**, *277*, 532.
(8) Teetsov, J.; Vanden Bout, D. A. *J. Am. Chem. Soc.* **2001**, *123*, 3605.
(9) Stevenson, R.; Riehn, R.; Milner, R. G.; Richards, D.; Moons, E.; Kang, D.-J.; Bramire, M.; Morgado, J.; Cacialli, F. *Appl. Phys. Lett.* **2001**, *79*, 833.
(10) Chappell, J.; Lidzey, D. G.; Jukes, P. C.; Higgins, A. M.; Thompson, R. L.; O'Connor, S.; Grizzi, I.; Fletcher, R.; O'Brien, J.; Geoghegan, M.; Jones, R. A. *Nat. Mater.* **2003**, *9*, 616.
(11) Cadby, A.; Dean, R.; Fox, A. M.; Jones, R. A. L.; Lidzey, D. G. *Nano Lett.* **2005**, *5*, 2232.
(12) Seidel, J.; Grafström, S.; Loppacher, Ch.; Trogisch, S.; Schlaphof, F.; Eng. L. M. *Appl. Phys. Lett.* **2001**, *79*, 2291.
(13) Mikhailovsky, A. A.; Petruska, M. A.; Stockman, M. I.; Klimov, V. I. *Opt. Lett.* **2003**, *28*, 1686.
(14) Mikhailovsky, A. A.; Petruska, M. A.; Li, K.; Stockman, M. I.; Klimov, V. I. *Phys. Rev. B* **2004**, *69*, 085401.
(15) Saito, T.; Sisk, W.; Kobayashi, T.; Suzuki, S.; Iwayanagi, T. *J. Phys. Chem.* **1993**, *97*, 8026.
(16) Yamashita, A.; Maruno, T.; Hayashi, T. *J. Phys. Chem.* **1993**, *97*, 4567.
(17) Yamashita, A.; Maruno, T.; Hayashi, T. *J. Phys. Chem.* **1994**, *98*, 12695.
(18) Peumans, P.; Uchida, S.; Forrest, S. R. *Nature* **2003**, *425*, 158.
(19) Tsuzuki, T.; Shirota, Y.; Rostalski, J.; Meissner, D. *Sol. Energy Mater. Sol. Cells* **2000**, *61*, 1.
(20) Diamant, Y.; Zaban, A. *J. Sol. Energy Eng.* **2004**, *126*, 893.
(21) Del Caño, T.; Parra, V.; Rodríguez-Méndez, M. L.; Aroca, R. F.; De Saja, J. A. *Appl. Surf. Sci.* **2005**, *246*, 327.
(22) Mizuguchi, J.; Rihs, G.; Karfunkel, H. R. *J. Phys. Chem.* **1995**, *99*, 16217.
(23) Hecht, B.; Bielefeldt, H.; Inouye, Y.; Pohl, D. W.; Novotny, L. J. *Appl. Phys.* **1997**, *81*, 2492.
(24) Lienau, C. *Philos. Trans. R. Soc. London, Ser. A* **2004**, *362*, 861.
(25) Stuebinger, T.; Bruetting, W. *J. Appl. Phys.* **2006**, *90*, 3632.
(26) Russel, P. *Science* **2003**, *299*, 358.
(27) Hillenbrand, R.; Keilmann, F. *Appl. Phys. Lett.* **2002**, *80*, 25.

NL070083I